CPLANE protein INTU regulates growth and patterning of the mouse lungs through cilia-dependent Hh signaling

Huiqing Zeng[1], Shimaa Ali[1, 2], Aswathy Sebastian[3], Adriana Sophia Ramos-Medero[1], Istvan Albert[3], Charlotte Dean[4] and Aimin Liu[1,*]

1. Department of Biology, Eberly College of Science, Huck Institute of Life Sciences, The Pennsylvania State University, University Park, PA 16802, USA
2. Faculty of Veterinary Medicine, Sohag University, Sohag, Egypt, 82524
3. Department of Biochemistry and Molecular Biology, Eberly College of Science, Huck Institute of Life Sciences, The Pennsylvania State University, University Park, PA 16802, USA
4. National Heart and Lung Institute, Imperial College London, London SW7 2AZ, UK

* Corresponding author: axl25@psu.edu

Abstract

Congenital lung malformations are fatal at birth in their severe forms. Prevention and early intervention of these birth defects require a comprehensive understanding of the molecular mechanisms of lung development. We find that the loss of *inturned* (*Intu*), a cilia and planar polarity effector gene, severely disrupts growth and branching morphogenesis of the mouse embryonic lungs. Consistent with our previous results indicating an important role for *Intu* in ciliogenesis and hedgehog (Hh) signaling, we find greatly reduced number of primary cilia in both the epithelial and mesenchymal tissues of the lungs. We also find significantly reduced expression of *Gli1* and *Ptch1*, direct targets of Hh signaling, suggesting disruption of cilia-dependent Hh signaling in *Intu* mutant lungs. An agonist of the Hh pathway activator, smoothened, increases Hh target gene expression and tubulogenesis in explanted wild type, but not *Intu* mutant, lungs, suggesting impaired Hh signaling response underlying lung morphogenetic defects in *Intu* mutants. Furthermore, removing both *Gli2* and *Intu* completely abolishes branching morphogenesis of the lung, strongly supporting a mechanism by which *Intu* regulates lung growth and patterning through cilia-dependent Hh signaling. Moreover, a transcriptomics analysis identifies around 200 differentially expressed genes (DEGs) in *Intu* mutant lungs, including known Hh target genes *Gli1, Ptch1/2* and *Hhip*. Genes involved in muscle differentiation and function are highly enriched among the DEGs, consistent with an important role of Hh signaling in airway smooth muscle differentiation. In addition, we find that the difference in gene expression between the left and right lungs diminishes in *Intu* mutants, suggesting an important role of *Intu* in asymmetrical growth and patterning of the mouse lungs.

Keywords: CPLANE; Intu; cilia; Hh signaling; lung; left/right asymmetry

Introduction

The lung is an organ of gas exchange indispensable for all mammals. Congenital lung malformations affect 30~42 per 100,000 people, and the most severe cases are incompatible with life (Andrade et al., 2011). The development of lungs involves tremendous amount of growth and complex branching morphogenesis of the airway epithelium (Metzger et al., 2008). It has been shown that the branching patterns of the airway epithelium, at least in the beginning, are highly stereotypical and appear to have a solid genetic basis (Metzger et al., 2008). Interactions between the branch tip epithelium and the surrounding mesenchyme are key to the proper development of the lung, and involve many well-known signaling pathways, including the retinoic acid, hedgehog (Hh), fibroblast growth factor (FGF), platelet-derived growth factor (PDGF), bone morphogenetic protein (BMP) and wingless-related integration site (Wnt) pathways (Herriges and Morrisey, 2014). Mechanical forces were also suggested as a contributor to the sculpture of the airway epithelial network (Goodwin and Nelson, 2020). However, exactly how these signaling pathways and various mechanical forces are integrated to ensure normal growth and branching of the airway epithelium remains enigmatic.

Although all mammals appear bilaterally symmetrical externally, asymmetry along the left/right (L/R) axis exists in the arrangement of internal organs including the lung (Grimes, 2019; Grimes and Burdine, 2017). In normal mice, the left lung comprises a single lobe, whereas the right lung comprises four morphologically distinct lobes, the cranial, middle, caudal and accessory lobes (Herriges and Morrisey, 2014). Earlier studies focused on the breaking of the embryonic L/R symmetry at the embryonic node, and the propagation of the asymmetrical signal to the lateral plate mesoderm (LPM; (Hamada and Tam, 2014). Recent studies have indicated that the LPM-derived signals guide the looping of the heart and gut tubes asymmetrically (Grimes, 2019; Grimes and Burdine, 2017). The L/R asymmetry of the lung is also induced by the LPM-derived signals (Grimes, 2019; Grimes and Burdine, 2017). However, the intrinsic molecular mechanisms in the lung that allow its proper response to the L/R patterning signals and subsequent differential development of the two sides have not been revealed.

Sonic hedgehog (SHH), an important member of the Hh family of signaling molecules, is expressed in the cells at the distal tips of airway epithelium, and is important for the growth and branching of the lung (Bellusci et al., 1996; Bitgood and McMahon, 1995; Pepicelli et al., 1998; Urase et al., 1996). Two transcription factors of the Glioma Associated Oncoprotein (GLI) family,

GLI2 and GLI3, work together in the initial induction and subsequent growth and branching of the lung (Grindley et al., 1997; Motoyama et al., 1998). SHH regulates lung morphogenesis at least partially through the regulation of other pathways, such as FGF10, WNT2/2b and BMP4 (Fernandes-Silva et al., 2017; Ludtke et al., 2016; Rankin et al., 2016).

The primary cilia are critical for many developmental processes in vertebrates (Oh and Katsanis, 2012). Mild lung growth and branching defects have been described in chicken and mouse mutants with partial loss of cilia (Davey et al., 2014; Goggolidou et al., 2014; Lee and Ko, 2020; Tong et al., 2017), but the early lethality of mutant mice suffered from complete cilia loss has hindered our understanding of the absolute requirement for the cilia in lung development. The ciliogenesis and planar polarity effector (CPLANE) protein inturned (INTU) is an important regulator of ciliogenesis (Agbu et al., 2018; Zeng et al., 2010). It regulates early patterning of the neural tube and limb buds through SHH signaling, and regulates cartilage and bone formation through Indian hedgehog (IHH, another Hh family member) signaling (Chang et al., 2015; Zeng et al., 2010). In addition to its role in embryonic development, INTU also regulates hair growth and promotes tissue repair in a kidney injury model (Dai et al., 2013; Wang et al., 2022; Wang et al., 2018). The *Intu* null mutant offers a unique opportunity to study the impact of severe loss of cilia on lung morphogenesis.

In the current study, we report a drastic reduction in the growth and branching of the embryonic lung, especially the right lung, in *Intu* null mutants. We further show defective ciliogenesis in both the epithelium and mesenchyme of the *Intu* mutant lungs. Hh target genes such as *Patched 1* (*Ptch1)* and *Gli1* were expressed at reduced levels in *Intu* mutant lungs, suggesting compromised Hh pathway activation. *Intu* mutant lung explants failed to increase Hh target gene expression and tubular morphogenesis in response to a smoothened agonist (SAG), suggesting that defective response to cilia-dependent Hh signaling underlies the *Intu* mutant lung phenotype. Through a transcriptomic approach, we find that genes associated with smooth muscle differentiation and those related to Hh signaling pathway were differentially expressed in *Intu* mutant lungs. Finally, we find multiple DEGs between the left and right wild type lungs, but the difference diminishes for the majority of these DEGs in *Intu* mutants, suggesting that *Intu* promotes bilateral asymmetry of the lung through regulating differential expression of downstream genes.

Results

Defective lung morphogenesis in Intu mutants

The development of lungs and the trachea is initiated with specific expression of NK2 homeobox 1 (Nkx2-1) in a patch of cells on the ventral side of the foregut, followed with outgrowth of two Nkx2-1-expressing side branches corresponding to the two future bronchi (Minoo et al., 1999). To precisely evaluate the initiation and progression of the embryonic lung development, we performed wholemount immunofluorescence analyses with an anti-Nkx2-1 antibody on wild type and *Intu* mutant lungs at E10.5. The primordia for the left and right bronchi could be seen as Nkx2-1 positive buds branched out from the caudal end of the wild type trachea (Fig. 1A). In contrast, Nkx2-1 expression was seen in an extended area on the ventral side of the foregut, and the bronchi primordia had not started or just started to grow in *Intu* mutants (Fig. 1A). At subsequent stages, we performed wholemount immunofluorescence analyses with an anti-cadherin 1 (CDH1) antibody to label epithelial cells. With this approach, we saw in the E11.5 wild type lungs all the primary branches, including the four lobes in the right lung, and some secondary branches (Fig. 1B). In contrast, the *Intu* mutant lungs just started to initiate primary branching at this stage, and it was clear that the accessary lobe was absent (Fig.1B). At E12.5, the wild type lungs had numerous secondary branches (Fig. 1C), whereas the *Intu* mutant lungs just started to initiate secondary branching (Fig. 1C). At E13.5, the last stage live *Intu* mutant embryos were recovered, it was clear that the *Intu* mutant lungs were significantly smaller than wild type lungs (Fig. 1D).

To quantify the lung morphogenetic defects in *Intu* mutants, we counted the numbers of branch tips to quantify the complexity of the lung branch network at E12.5. We found on average a 3-fold reduction of branch tips in the left lungs, and a 7-fold reduction in the right lungs (Fig. 1E), suggesting severe branching morphogenetic defects in *Intu* mutant lungs.

Not only the size and complexity of the *Intu* mutant lungs were greatly reduced compared to control lungs, but their branching patterns were also altered. First, the accessory lobe was absent in all *Intu* mutant lungs, whereas the other lobes in the right lung fused into one single lobe (better appreciated in Fig. 1D). Second, the branching pattern in the right lung was more complex than that of the left in control lungs, but this difference diminished in *Intu* mutants (Fig. 1E). Finally, primary lung branches form in a proximal-to-distal order, and lateral branches form prior to dorsal

and ventral branches (Fig. 1F and (Metzger et al., 2008). We found that dorsal and ventral branches formed prematurely in *Intu* mutant lungs, and sometimes starting in a distal rather than proximal location (Fig. 1F). This suggests that signals instructing the stereotypical lung branching pattern were not functioning properly in *Intu* mutants.

Reduced ciliogenesis and Hh signaling in the Intu mutant lungs

Our previous work indicated an important role for *Intu* in ciliogenesis and Hh signaling in central nervous system, skin and skeleton (Chang et al., 2015; Dai et al., 2013; Zeng et al., 2010). To test whether it plays a similar role in lung development, we first examined ciliogenesis in lung tubules and surrounding mesenchyme at E12.5 through immunofluorescence of a cilia-specific protein, ARL13B (Fig. 2). As expected, the ciliation frequency in the *Intu* mutant lung tubules (18.4%) was significantly lower than that in wild type (86.8%) (Fig. 2). Similar reduction in ciliogenesis was also observed for the surrounding mesenchyme, where 53.1% of wild type cells grew cilia, but only 20.1% of *Intu* mutant cells grew cilia (Fig. 2).

As Hh signaling in mammals is cilia-dependent (Huangfu et al., 2003; Liu et al., 2005), and SHH and its downstream effector GLI transcription factors were known to regulate lung development (Motoyama et al., 1998; Pepicelli et al., 1998), we set out to determine whether Hh signaling in *Intu* mutant lungs was compromised as the result of reduced ciliogenesis. Through wholemount RNA in situ hybridization, we found similar patterns of *Shh* expression in the distal regions of the tubules in wild type and *Intu* mutant lungs (Fig. 3A, B). In contrast, *Ptch1*, a known transcriptional readout of the Hh signaling, was expressed at a reduced level in the mesenchyme compared to wild type, suggesting a disruption of signal transduction downstream of SHH (Fig. 3C, D). This Hh signaling defect was also reflected in reduced expression of two Hh pathway reporter genes, *Ptch1-lacZ* and *Gli1-lacZ* (Fig. 3E-H). To quantify the levels of Hh pathway activation, we examined the expression of *Ptch1* and *Gli1* through quantitative reverse transcriptase polymerase chain reaction (qRT-PCR), and found a significant decrease in the expression of both genes in E12.5 *Intu* mutant left and right lungs compared to their wild type littermates (Fig. 3I). We also found significant reduction of *Ptch1* and *Gli1* expression in E12.5 *Intu* mutant lungs compared to E11.5 wild type lungs, which are similar in size and branching complexity, suggesting that the decrease in Hh target gene expression was not due to delayed development or reduced complexity in branching patterns of the *Intu* mutant lungs (Fig. 3I).

Hh pathway activation promotes tubulogenesis in wild type, but not in Intu mutant lung explants

The reduction in ciliogenesis and Hh signaling in *Intu* mutant lungs raised the possibility that *Intu* regulates lung tubulogenesis through cilia-dependent Hh signaling. To test this hypothesis, we cultured E11.5 lung explants following a published protocol (Dean et al., 2005). We found that treating the wild type lung explants with an agonist for smoothened (SAG), a positive regulator of Hh signaling, drastically increased expression of *Gli1-lacZ* (Fig. 4A) and *Ptch1-lacZ* (Fig. 4B), two Hh signaling indicators. In contrast, SAG treatment of the *Intu* mutant lung explants failed to increase either reporter expression (Fig. 4A and B). Moreover, cysts developed in distal parts of both solvent-treated wild type and *Intu* mutant lung explants (Fig. 4C), and SAG inhibited cyst formation and promoted tubular growth and branching in wild type lung explants (Fig. 4C, D). Strikingly, treating *Intu* mutant lung explants with SAG failed to inhibit cystogenesis or promote growth and branching (Fig. 4C, D). These results suggest that *Intu*-dependent cellular response to SHH is critical for tubulogenesis in the lung.

GLI2 degradation and GLI3 processing are compromised in Intu mutant lungs

Both GLI2 and GLI3 are substrates of β–TRCP (β transducin repeat containing protein) ubiquitin ligase, which targets GLI2 for degradation and full-length GLI3 (GLI3FL) for processing into a smaller repressor form (GLI3R) (Pan and Wang, 2007). We have previously shown compromised GLI3 processing in E10.5 *Intu* mutant whole embryos (Zeng et al., 2010), and set out to determine whether *Intu* similarly regulates GLI3 processing, and whether it is involved in GLI2 degradation in the lung. We found a significant increase in the level of GLI2 protein in E13.5 *Intu* mutant lungs, suggesting that *Intu* indeed regulates GLI2 degradation (Fig. 5A and B). We also found significant increases in the amount of GLI3FL and the ratio between GLI3FL and GLI3R, along with a slight and insignificant decrease in the level of GLI3R, suggesting compromised GLI3 processing in the lung (Fig. 5A, C~E).

Intu genetically interacts with Gli2 in lung morphogenesis

To further test the hypothesis that *Intu* regulates lung morphogenesis through cilia-dependent Hh signaling, we investigated the genetic interaction between *Intu* and *Gli2*. Although GLI2 is the primary activator of the Hh pathway, E12.5 *Gli2* mutant embryos did not look

drastically different from wild type littermates (compare Fig. 6A and B). *Intu* mutants, on the other hands, exhibited multiple morphological defects in the brain, craniofacial structures, heart and the limb buds (Fig. 6C; (Zeng et al., 2010). *Intu;Gli2* double mutants exhibited more severe neural tube and heart defects than *Intu* mutants, but did not appear severely delayed or arrested at an earlier stage (Fig. 6D). *Gli2* mutant lungs lost the right accessory lobe, and the remaining right lung lobes fused into a single one (compare Fig. 6E and F; (Matise and Joyner, 1999; Motoyama et al., 1998). Loss of *Intu* alone leads to similar loss of lobes in the right lung, and more severe branching defects than *Gli2* mutants (Fig. 6G). This likely reflects the roles of GLI3 activator that requires activation inside the cilia, as it has been shown that $Gli2^{-/-};Gli3^{+/-}$ mutants exhibited more severe lung branching defects than *Gli2* mutants (Motoyama et al., 1998). Interestingly, loss of both *Intu* and *Gli2* results in the loss of lung branching completely (Fig. 6H). In these double mutants, *Nkx2-1* expression was initiated on the ventral side of the foregut, but the *Nkx2-1* expressing cells failed to detach from the foregut to form the trachea or form branches to either left or right side (Fig. 6H). This more severe phenotype in double mutants than either *Gli2* or *Intu* single mutants suggests that the branching morphogenesis defects in *Intu* mutants result from compromised GLI activities.

A transcriptomic analysis revealed the roles of Intu in asymmetrical lung development and smooth muscle differentiation

To reach an unbiased understanding of the molecular impact of loss of *Intu* on lung development, we performed transcriptomic analyses on E12.5 wild type and *Intu* mutant lungs. As loss of *Intu* appears to have asymmetrical impacts on the left and right lungs, we analyzed the two sides separately. A principal component analysis (PCA) of the sequencing results indicated a clear difference between the transcriptomes of the wild type and *Intu* mutant lungs (Fig. 7A). It also indicated more variation among *Intu* mutant lungs compared to that among wild type lungs, which was consistent with our observation that the severity of the *Intu* mutant lung phenotype was variable. As expected, downregulation of known Hh pathway target genes such as *Gli1*, *Hhip (Hedgehog-interacting protein), Ptch1* and *Ptch2* in *Intu* mutants was detected, proving the sensitivity of the assay (Fig. 7B and C). In total, 200 genes were identified as differentially expressed genes (DEGs) between wild type and *Intu* mutant lungs (Fig. 7C; Supplemental tables 1 and 2). Many DEGs (n=86) were identified in both left and right lungs. Consistent with the right

lung being more affected in *Intu* mutants, more DEGs were identified in the right lungs only (n=80) than in the left lungs only (n=34).

Interestingly, 17 genes were expressed differentially between the wild type left and right lungs, suggesting intrinsic molecular programs underlying asymmetrical development (Supplemental table 3). In contrast, only three genes were differentially expressed between *Intu* mutant left and right lungs, suggesting an important role of *Intu* in regulating asymmetrical development of the lungs through differential expression of genes. The PCA analysis also revealed the decrease in bilateral asymmetry as the left and right lungs overlap more in *Intu* mutants (Fig. 7A). One of the genes that was expressed at a higher level in the left lungs of both wild type (5 fold difference) and *Intu* mutant (10 fold difference) lungs was *Pitx2*, a known regulator of left/right asymmetry in lateral plate mesoderm (Yoshioka et al., 1998). Another such DEG was *Hoxa6*, which was expressed at higher levels in the right lungs of wild type (2.4-fold) and *Intu* mutant (1.7-fold). This suggests that the loss of asymmetry in the *Intu* mutant lungs is due to intrinsic changes in the lung, not secondary to an earlier defect in the node or lateral plate mesoderm.

Gene Ontology analysis indicated cytoskeletal protein binding, movement of cell or subcellular component, animal organ morphogenesis, regulation of cell population proliferation and Hh signaling pathway as biological processes significantly affected by loss of *Intu* (Fig. 7D). These were consistent with our observation of the morphogenetic defects in lung development, and abnormal Hh signaling in *Intu* mutants. The enrichment of genes involved in cytoskeletal protein binding and movement of cell or subcellular components was consistent with a role of Hh signaling in promoting smooth muscle differentiation (Miller et al., 2004). In fact, at least 19 DEGs downregulated in *Intu* mutant lungs, such as myocardin (*Myocd*), smooth muscle actin (*Acta2*), myosin light chain 9 (*Myl9*) and heavy chain 11 (*Myh11*) were known to be expressed in smooth muscle cells (Fig. 7E)(Chen et al., 2002; Huang et al., 2022; Leslie et al., 1990; Matsuoka et al., 1993).

Smooth muscle differentiation and IGF-1 signaling were compromised in Intu mutant lungs

To better understand the molecular and cellular mechanisms by which *Intu* regulates lung morphogenesis, we examined the expression of several DEGs identified in our transcriptomic profile analysis. We first examined the transcription factor forkhead box F1 (*Foxf1)*, which was a

known essential regulator of lung development and downstream target of Hh signaling (Lim et al., 2002; Mahlapuu et al., 2001; Ustiyan et al., 2018). RNA in situ hybridization showed strong *Foxf1* expression in wild type lung mesenchyme, and it was greatly downregulated in *Intu* mutants (Fig. 8A). qRT-PCR confirmed that *Foxf1* transcript level in E12.5 *Intu* mutant lungs is significantly lower than those in E11.5 or E12.5 wild type lungs, suggesting that the difference was not due to difference in size or complexity of the lungs (Fig. 8A). Consistent with previous studies showing crucial roles of *Shh* and *Foxf1* in airway smooth muscle lineage formation in the lungs, we found less smooth muscle actin staining in *Intu* mutant lungs (Fig. 8B). Another DEG identified from our transcriptomic analysis was insulin growth factor-1 (*Igf1*), which has been shown to promote embryonic lung growth (Epaud et al., 2012). By RNA in situ hybridization and qRT-PCR, we found that the lung specific expression of *Igf1* was significantly reduced in *Intu* mutants, suggesting compromised IGF signaling may contribute to the growth defects in *Intu* mutant lung (Fig. 8C).

Discussion

In the current study, we report severe growth and patterning defects in the lungs of a null mutant of the CPLANE gene *Intu*. We show a significant reduction of cilia in both the lung tubules and surrounding mesenchyme, as well as a decrease in Hh signaling activities. We demonstrated the important roles of cilia-dependent Hh signaling downstream of *Intu* by showing the loss of tubulogenic effect of a smoothened agonist on *Intu* mutant lung explants, and by showing the synergistic interaction between *Intu* and *Gli2* in double mutants. By profiling the transcriptomes, we identified Hh signaling and smooth muscle formation as key downstream processes regulated by *Intu,* which we confirmed by RNA in situ hybridization, immunofluorescence and qRT-PCR analyses. We also found a diminished difference in both morphology and gene expression between the left and right lungs in the *Intu* mutants, suggesting a potential role for *Intu* in mediating asymmetrical development of this important organ.

The lung morphogenetic defects in *Intu* mutants coincide with compromised cilia-dependent Hh signaling. Is this simply a coincidence or do the morphogenetic defects in *Intu* mutants result from compromised Hh signaling? We provide strong evidence for the latter. First, our *in vitro* explant study indicates that activating Hh signaling with a SMO agonist promotes tubulogenesis in wild type, but not in *Intu* mutants, suggesting that *Intu* mediates the tubulogenic

effects of Hh signaling by regulating cellular responses to Hh pathway activation. Furthermore, *Intu* genetically interacts with *Gli2*, suggesting that compromised GLI activity is responsible for defects in branching morphogenesis in *Intu* mutant lungs. Therefore, these functional assays support compromised cilia-dependent Hh signaling as the underlying cause for the lung morphogenetic defects in *Intu* mutants.

It has been reported that simultaneous loss of both *Gli2* and *Gli3* leads to the complete absence of lungs (Motoyama et al., 1998). *Intu* mutant lungs exhibit similar, but more severe, lung defects than *Gli2*$^{-/-}$ mutant lungs, suggesting that both GLI2 and GLI3 activators are compromised in *Intu* mutants. It is also worth noting that *Gli2;Intu* double mutants exhibit more severe lung defects than *Shh* mutants, which develop some primary branches but fail to undergo normal tubulogenesis, ending up with large cysts (Pepicelli et al., 1998). One possible explanation for this difference is that other Hh ligands, such as IHH, may partially compensate for the loss of *Shh*. On the other hand, severe loss of cilia in *Intu* mutants disrupts cellular response to both SHH and IHH (Chang et al., 2015; Zeng et al., 2010).

Recent reports linked kinases (cyclin-dependent kinase 20 and ciliogenesis associated kinase 1) regulating the length of cilia to lung growth and patterning, but it remained unclear whether the lung phenotype in these mutants reflect a requirement for the cilia or other potential functions of the affected enzymes (Lee and Ko, 2020; Tong et al., 2017). The mechanisms by which CPLANE proteins, such as INTU, regulate ciliogenesis are clearer, and *Intu* null mutant provides the best possible model for the function of cilia in lung development (Adler and Wallingford, 2017). Compared to previous reports, we find more severe impact of *Intu* mutation on lung development, suggesting that cilia play more important roles in lung development than previously appreciated. It is worth noting that a small number of cilia are still present in *Intu* mutant lungs, suggesting that lung development may be more disrupted should all cilia be removed. Unfortunately, embryos with no cilia, such as *Ift88* null, die earlier, preventing a thorough analysis of lung development (Murcia et al., 2000). Therefore, a conditional approach may be needed in the future to reveal the true requirement for cilia in lung development.

Our gene expression analysis indicates significant decrease in genes associated with smooth muscle development. This is consistent with previous studies indicating that smooth muscle development is dependent on Hh signaling (Miller et al., 2004; Weaver et al., 2003). It remains controversial whether this smooth muscle developmental defect leads directly to lung

branching defects. Studies using explants and microfluidic devices showed that smooth muscle helped to sculpt lung branches (Jaslove et al., 2022; Nelson et al., 2017). In contrast, genetic ablations of smooth muscle differentiation or function have failed to reproduce the kind of lung branching defects of Hh pathway mutants or *Intu* mutants (Young et al., 2020). It would be helpful to determine whether restoring smooth muscle differentiation could rescue lung development in *Gli2* or *Intu* mutants.

Mammalian left/right patterning is initiated at the embryonic node, propagated to the lateral plate mesoderm, and ultimately results in asymmetrical positioning/morphogenesis of organs such as the lung (Hamada, 2020). Much has been learned about the signaling cascade from the node to the lateral plate mesoderm, but little was known on how these signals were translated into asymmetrical organ placement/morphology. It is interesting that the right lung is more severely affected in the *Intu* mutants, leading to diminished asymmetry between the two sides. Our transcriptomic analysis indicates that paired-like homeodomain transcription factor 2 *(Pitx2)*, a left/right determinant in the lateral plate mesoderm, remains asymmetrically expressed in the left lung of *Intu* mutants, suggesting that the left/right defects in *Intu* mutant lungs does not result from a failure in setting up the overall left/right asymmetry in the node or lateral plate mesoderm (Yoshioka et al., 1998). Interestingly, we find that most genes asymmetrically expressed in wild type lungs are no longer asymmetrically expressed in *Intu* mutants, suggesting that *Intu* promotes lung asymmetry by differentially regulating the expression of these genes. It will be interesting to study the detailed transcriptional regulation mechanism that leads to such difference.

In conclusion, we have revealed important roles of *Intu* and primary cilia in mouse lung growth, branching morphogenesis, as well as asymmetrical morphogenesis between the left and right lungs. This knowledge will allow us to better understand how ciliopathy impacts morphogenesis, and will likely benefit the effort in prevention and intervention of these defects.

Materials and methods

Mice

The following mouse strains, *Gli1*^{tm2Alj}, *Gli2*$^{tm2.1Alj}$ (Bai and Joyner, 2001), *Intu*$^{tm1.2Aliu}$ (Zeng et al., 2010) and *Ptch1*^{tm2Mps} (Goodrich et al., 1997), were kept on C57BL/6Tac background and genotyped according to published protocols. The use of the animals in this work was approved by the IACUC at Penn State University.

Wholemount immunofluorescence

Lungs were dissected at specific embryonic stages (E10~E13) in ice-cold phosphate buffered saline (PBS), and fixed in 4% paraformaldehyde (PFA) on ice for 30 minutes. They were then washed in PBS plus 0.1% Triton X-100 (PBST) three times and then incubated with primary antibodies overnight at 4°C. On the next day, they were again washed three times with PBST and incubated with AlexaFluor 488-conjugated secondary antibodies at 4°C overnight. On the third day, they were washed three more times with PBST and photos were taken using a Zeiss Discovery Microscope and a QImaging micropublisher camera. Primary antibodies used were against E-cadherin (Sigma, U3254) and Nkx2-1 (Epitomics, 2044-1).

Lung explant culture

Lungs were dissected at E11.5 in ice-cold PBS, and cultured at the liquid/air interface on Nuclepore filters (Whatman, 110414) floating on BGjb medium (Thermofisher Scientific) containing 100nM smoothened agonist (SAG) or 0.5% DMSO for 48 hrs at 37°C and 5% CO_2. By the end of the culture, the explants were fixed in 4% PFA on ice for 30 minutes and proceeded with wholemount immunofluorescence, Xgal staining or RNA in situ hybridization.

Wholemount Xgal staining

Lightly fixed Lungs or explants were washed in Xgal wash buffer (PBS plus 2mM $MgCl_2$, 0.01% sodium deoxycholate and 0.02% NP40) three times and incubated with Xgal staining solution (1mg/ml Xgal, potassium ferrocyanide and potassium ferricyanide in wash buffer) at 37°C overnight, washed three times with PBS and postfixed in 4% PFA overnight. Photos were taken on a Zeiss Discovery Microscope and a QImaging micropublisher camera.

Wholemount RNA in situ hybridization

Lungs or explants were fixed for at least four hours in 4% PFA at 4°C, treated with proteinase K, postfixed briefly in 4% PFA and then incubated with Digoxigenin RNA probes overnight at 70°C. On the following day, samples were washed, treated with RNaseA, blocked with BM blocking reagent (Roche) and incubated with an anti-Digoxigenin antibody at 4°C overnight. On the third day, samples were washed extensively with Maleic Acid Buffer and then incubated with BM purple (Roche) in the dark until the signals were good. The samples were then washed with PBS plus 0.1% Tween20 and photos were taken with a Zeiss Discovery Microscope and a QImaging micropublisher camera.

Immunoblot Analyses

Whole cell protein lysates were prepared, separated on SDS polyacrylamide gel and transferred to nitrocellulose membrane according to a previously described protocol (Zeng et al., 2010). After primary antibody incubation, membranes were incubated with IRD680- and IRD800-conjugated secondary antibodies (LI-COR), and scanned on a LI-COR Odyssey CLx imaging system. Quantitative analysis was performed using Image Studio (LI-COR). Primary antibodies used: GLI2 (R&D Systems), GLI3(R&D Systems) and β-tubulin (Sigma-Aldrich).

RNA preparation, RT-PCR and RNA sequencing

RNA was extracted from freshly dissected lungs using a NucleoSpin RNA miniprep kit (Macherey-Nagel). cDNA was synthesized using qScript cDNA SuperMix (Quanta Biosciences). PCR reactions were performed using a StepOnePlus Real-time PCR system (Applied Biosystems). All samples were analyzed in triplicates and normalized to the housekeeping gene *Gapdh*. Primers used for qRT-PCR were: *Gli1*, 5′-CGTTTGAAGGCTGTCGGAAG-3′ and 5′-GCGTCTTGAGGTTTTCAAGGC-3′. *Ptch1*, 5’-CTCCAAGTGTCGTCCGGTTT-3’ and 5’-ACCCATTGTTCGTGTGACCA-3’, *Foxf1*: 5’-CTGGAGCAGCCATACCTTCAC-3’ and 5’-CGAGGGATGCCTTGCAGTT-3’, *Igf1*, 5’-GCCCCACTGAAGCCTACAAA-3’ and 5’-TGAGTCTTGGGCATGTCAGTGT-3’. *Gapdh*, 5’-GTCGGTGTGAACGGATTTGG-3’ and 5’-GACTCCACGACATACTCAGC-3’. The specificity of the primers was tested on null mutant embryos lacking target gene transcription and/or on cells overexpressing GFP-tagged target genes.

For RNA sequencing, RNA samples were submitted to BGI Genomics on dry ice for non-stranded mRNA sequencing on a DNBseq platform. On average 47 million clean reads were generated for each sample. FastQC reports were generated, and the data quality was inspected. Data was mapped to the mouse refence genome (GRCm38 build) using HISAT2. About 98% of the data were mapped to the reference genome. The number of reads mapped to the annotated genes were obtained using featureCounts in the unstranded and paired mode (-p -s 0 parameters). Differentially expressed genes across different conditions were obtained using DESeq2 and edgeR packages in R following the recommended protocol. PCA and pathway analyses were performed, and volcano plot and heatmap were generated in R. Gene ontology analysis was performed through g:Profiler (http://biit.cs.ut.ee/gprofiler/gost). The raw and processed data files with associated metadata have been submitted to NIH Gene Expression Omnibus with accession #GSE251669.

Statistical Analyses

Student's t-tests were performed using *Graphpad Prism 10.2.3*. Outliers were identified and excluded based on the 1.5xIQR rule using *MS Excel*.

Acknowledgement

We thank Drs McMahon, Scott and Joyner for RNA in situ hybridization probes. We also thank Drs. Bai, Joyner and Scott for *Gli1-lacZ*, *Gli2* and *Ptch1-lacZ* mouse strains. This research is supported by NIH (R03HD102462), an Egyptian government scholarship for S.A., a Penn State new lab start up fund and undergrad support for A.S.R-M. by NASA space grant consortium.

References:

Adler, P.N., Wallingford, J.B., 2017. From Planar Cell Polarity to Ciliogenesis and Back: The Curious Tale of the PPE and CPLANE proteins. Trends Cell Biol 27, 379-390.

Agbu, S.O., Liang, Y., Liu, A., Anderson, K.V., 2018. The small GTPase RSG1 controls a final step in primary cilia initiation. J Cell Biol 217, 413-427.

Andrade, C.F., Ferreira, H.P., Fischer, G.B., 2011. Congenital lung malformations. J Bras Pneumol 37, 259-271.

Bai, C.B., Joyner, A.L., 2001. Gli1 can rescue the in vivo function of Gli2. Development 128, 5161-5172.

Bellusci, S., Henderson, R., Winnier, G., Oikawa, T., Hogan, B.L., 1996. Evidence from normal expression and targeted misexpression that bone morphogenetic protein (Bmp-4) plays a role in mouse embryonic lung morphogenesis. Development 122, 1693-1702.
Bitgood, M.J., McMahon, A.P., 1995. Hedgehog and Bmp genes are coexpressed at many diverse sites of cell-cell interaction in the mouse embryo. Dev Biol 172, 126-138.
Chang, R., Petersen, J.R., Niswander, L.A., Liu, A., 2015. A hypomorphic allele reveals an important role of inturned in mouse skeletal development. Dev Dyn 244, 736-747.
Chen, J., Kitchen, C.M., Streb, J.W., Miano, J.M., 2002. Myocardin: a component of a molecular switch for smooth muscle differentiation. J Mol Cell Cardiol 34, 1345-1356.
Dai, D., Li, L., Huebner, A., Zeng, H., Guevara, E., Claypool, D.J., Liu, A., Chen, J., 2013. Planar cell polarity effector gene Intu regulates cell fate-specific differentiation of keratinocytes through the primary cilia. Cell Death Differ 20, 130-138.
Davey, M.G., McTeir, L., Barrie, A.M., Freem, L.J., Stephen, L.A., 2014. Loss of cilia causes embryonic lung hypoplasia, liver fibrosis, and cholestasis in the talpid3 ciliopathy mutant. Organogenesis 10, 177-185.
Dean, C.H., Miller, L.A., Smith, A.N., Dufort, D., Lang, R.A., Niswander, L.A., 2005. Canonical Wnt signaling negatively regulates branching morphogenesis of the lung and lacrimal gland. Dev Biol 286, 270-286.
Epaud, R., Aubey, F., Xu, J., Chaker, Z., Clemessy, M., Dautin, A., Ahamed, K., Bonora, M., Hoyeau, N., Flejou, J.F., Mailleux, A., Clement, A., Henrion-Caude, A., Holzenberger, M., 2012. Knockout of insulin-like growth factor-1 receptor impairs distal lung morphogenesis. PLoS One 7, e48071.
Fernandes-Silva, H., Correia-Pinto, J., Moura, R.S., 2017. Canonical Sonic Hedgehog Signaling in Early Lung Development. J Dev Biol 5.
Goggolidou, P., Stevens, J.L., Agueci, F., Keynton, J., Wheway, G., Grimes, D.T., Patel, S.H., Hilton, H., Morthorst, S.K., DiPaolo, A., Williams, D.J., Sanderson, J., Khoronenkova, S.V., Powles-Glover, N., Ermakov, A., Esapa, C.T., Romero, R., Dianov, G.L., Briscoe, J., Johnson, C.A., Pedersen, L.B., Norris, D.P., 2014. ATMIN is a transcriptional regulator of both lung morphogenesis and ciliogenesis. Development 141, 3966-3977.
Goodrich, L.V., Milenkovic, L., Higgins, K.M., Scott, M.P., 1997. Altered neural cell fates and medulloblastoma in mouse patched mutants. Science 277, 1109-1113.
Goodwin, K., Nelson, C.M., 2020. Branching morphogenesis. Development 147.
Grimes, D.T., 2019. Making and breaking symmetry in development, growth and disease. Development 146.
Grimes, D.T., Burdine, R.D., 2017. Left-Right Patterning: Breaking Symmetry to Asymmetric Morphogenesis. Trends Genet 33, 616-628.
Grindley, J.C., Bellusci, S., Perkins, D., Hogan, B.L., 1997. Evidence for the involvement of the Gli gene family in embryonic mouse lung development. Dev Biol 188, 337-348.
Hamada, H., 2020. Molecular and cellular basis of left-right asymmetry in vertebrates. Proc Jpn Acad Ser B Phys Biol Sci 96, 273-296.
Hamada, H., Tam, P.P., 2014. Mechanisms of left-right asymmetry and patterning: driver, mediator and responder. F1000Prime Rep 6, 110.
Herriges, M., Morrisey, E.E., 2014. Lung development: orchestrating the generation and regeneration of a complex organ. Development 141, 502-513.

Huang, C.H., Schuring, J., Skinner, J.P., Mok, L., Chong, M.M.W., 2022. MYL9 deficiency is neonatal lethal in mice due to abnormalities in the lung and the muscularis propria of the bladder and intestine. PLoS One 17, e0270820.
Huangfu, D., Liu, A., Rakeman, A.S., Murcia, N.S., Niswander, L., Anderson, K.V., 2003. Hedgehog signalling in the mouse requires intraflagellar transport proteins. Nature 426, 83-87.
Jaslove, J.M., Goodwin, K., Sundarakrishnan, A., Spurlin, J.W., Mao, S., Kosmrlj, A., Nelson, C.M., 2022. Transmural pressure signals through retinoic acid to regulate lung branching. Development 149.
Lee, H., Ko, H.W., 2020. Cell cycle-related kinase is a crucial regulator for ciliogenesis and Hedgehog signaling in embryonic mouse lung development. BMB Rep.
Leslie, K.O., Mitchell, J.J., Woodcock-Mitchell, J.L., Low, R.B., 1990. Alpha smooth muscle actin expression in developing and adult human lung. Differentiation 44, 143-149.
Lim, L., Kalinichenko, V.V., Whitsett, J.A., Costa, R.H., 2002. Fusion of lung lobes and vessels in mouse embryos heterozygous for the forkhead box f1 targeted allele. Am J Physiol Lung Cell Mol Physiol 282, L1012-1022.
Liu, A., Wang, B., Niswander, L.A., 2005. Mouse intraflagellar transport proteins regulate both the activator and repressor functions of Gli transcription factors. Development 132, 3103-3111.
Ludtke, T.H., Rudat, C., Wojahn, I., Weiss, A.C., Kleppa, M.J., Kurz, J., Farin, H.F., Moon, A., Christoffels, V.M., Kispert, A., 2016. Tbx2 and Tbx3 Act Downstream of Shh to Maintain Canonical Wnt Signaling during Branching Morphogenesis of the Murine Lung. Dev Cell 39, 239-253.
Mahlapuu, M., Enerback, S., Carlsson, P., 2001. Haploinsufficiency of the forkhead gene Foxf1, a target for sonic hedgehog signaling, causes lung and foregut malformations. Development 128, 2397-2406.
Matise, M.P., Joyner, A.L., 1999. Gli genes in development and cancer. Oncogene 18, 7852-7859.
Matsuoka, R., Yoshida, M.C., Furutani, Y., Imamura, S., Kanda, N., Yanagisawa, M., Masaki, T., Takao, A., 1993. Human smooth muscle myosin heavy chain gene mapped to chromosomal region 16q12. Am J Med Genet 46, 61-67.
Metzger, R.J., Klein, O.D., Martin, G.R., Krasnow, M.A., 2008. The branching programme of mouse lung development. Nature 453, 745-750.
Miller, L.A., Wert, S.E., Clark, J.C., Xu, Y., Perl, A.K., Whitsett, J.A., 2004. Role of Sonic hedgehog in patterning of tracheal-bronchial cartilage and the peripheral lung. Dev Dyn 231, 57-71.
Minoo, P., Su, G., Drum, H., Bringas, P., Kimura, S., 1999. Defects in tracheoesophageal and lung morphogenesis in Nkx2.1(-/-) mouse embryos. Dev Biol 209, 60-71.
Motoyama, J., Liu, J., Mo, R., Ding, Q., Post, M., Hui, C.C., 1998. Essential function of Gli2 and Gli3 in the formation of lung, trachea and oesophagus. Nat Genet 20, 54-57.
Murcia, N.S., Richards, W.G., Yoder, B.K., Mucenski, M.L., Dunlap, J.R., Woychik, R.P., 2000. The Oak Ridge Polycystic Kidney (orpk) disease gene is required for left-right axis determination. Development 127, 2347-2355.
Nelson, C.M., Gleghorn, J.P., Pang, M.F., Jaslove, J.M., Goodwin, K., Varner, V.D., Miller, E., Radisky, D.C., Stone, H.A., 2017. Microfluidic chest cavities reveal that transmural pressure controls the rate of lung development. Development 144, 4328-4335.

Oh, E.C., Katsanis, N., 2012. Cilia in vertebrate development and disease. Development 139, 443-448.
Pan, Y., Wang, B., 2007. A novel protein-processing domain in Gli2 and Gli3 differentially blocks complete protein degradation by the proteasome. J Biol Chem 282, 10846-10852.
Pepicelli, C.V., Lewis, P.M., McMahon, A.P., 1998. Sonic hedgehog regulates branching morphogenesis in the mammalian lung. Curr Biol 8, 1083-1086.
Rankin, S.A., Han, L., McCracken, K.W., Kenny, A.P., Anglin, C.T., Grigg, E.A., Crawford, C.M., Wells, J.M., Shannon, J.M., Zorn, A.M., 2016. A Retinoic Acid-Hedgehog Cascade Coordinates Mesoderm-Inducing Signals and Endoderm Competence during Lung Specification. Cell Rep 16, 66-78.
Tong, Y., Park, S.H., Wu, D., Xu, W., Guillot, S.J., Jin, L., Li, X., Wang, Y., Lin, C.S., Fu, Z., 2017. An essential role of intestinal cell kinase in lung development is linked to the perinatal lethality of human ECO syndrome. FEBS Lett 591, 1247-1257.
Urase, K., Mukasa, T., Igarashi, H., Ishii, Y., Yasugi, S., Momoi, M.Y., Momoi, T., 1996. Spatial expression of Sonic hedgehog in the lung epithelium during branching morphogenesis. Biochem Biophys Res Commun 225, 161-166.
Ustiyan, V., Bolte, C., Zhang, Y., Han, L., Xu, Y., Yutzey, K.E., Zorn, A.M., Kalin, T.V., Shannon, J.M., Kalinichenko, V.V., 2018. FOXF1 transcription factor promotes lung morphogenesis by inducing cellular proliferation in fetal lung mesenchyme. Dev Biol 443, 50-63.
Wang, S., Liu, A., Su, Y., Dong, Z., 2022. Deficiency of the Planar Cell Polarity Protein Intu Delays Kidney Repair and Suppresses Renal Fibrosis after Acute Kidney Injury. Am J Pathol.
Wang, S., Liu, A., Wu, G., Ding, H.F., Huang, S., Nahman, S., Dong, Z., 2018. The CPLANE protein Intu protects kidneys from ischemia-reperfusion injury by targeting STAT1 for degradation. Nat Commun 9, 1234.
Weaver, M., Batts, L., Hogan, B.L., 2003. Tissue interactions pattern the mesenchyme of the embryonic mouse lung. Dev Biol 258, 169-184.
Yoshioka, H., Meno, C., Koshiba, K., Sugihara, M., Itoh, H., Ishimaru, Y., Inoue, T., Ohuchi, H., Semina, E.V., Murray, J.C., Hamada, H., Noji, S., 1998. Pitx2, a bicoid-type homeobox gene, is involved in a lefty-signaling pathway in determination of left-right asymmetry. Cell 94, 299-305.
Young, R.E., Jones, M.K., Hines, E.A., Li, R., Luo, Y., Shi, W., Verheyden, J.M., Sun, X., 2020. Smooth Muscle Differentiation Is Essential for Airway Size, Tracheal Cartilage Segmentation, but Dispensable for Epithelial Branching. Dev Cell 53, 73-85 e75.
Zeng, H., Hoover, A.N., Liu, A., 2010. PCP effector gene Inturned is an important regulator of cilia formation and embryonic development in mammals. Dev Biol 339, 418-428.

Figure legends:

Figure 1. Morphogenetic defects in *Intu* mutants lungs. (A) Dark field and NKX2-1 immunofluorescent images comparing wild type (n=10) and *Intu* mutant (n=8) lungs at E10.5. T: trachea; R: right; L: left. (B-D) Dark field and CDH1 immunofluorescent images comparing wild type and *Intu* mutant lungs at E11.5 (n=5 wild type and 3 mutant), E12.5 (n=7 wild type and 7 mutant) and E13.5 (n=6 wild type and 3 mutant). All images in A-D are ventral views. Dashed line in B outlines the lung. (E) Fewer branches formed in *Intu* mutant lungs. ***: $p<0.001$; ****: $p<0.0001$; unpaired, two-tailed *Student*'s t-test assuming unequal variances. (F) CDH1 immunofluorescent images of E12.5 wild type and *Intu* mutant lungs are shown in both ventral and dorsal views. The branching patterns are listed below the images with the primary and corresponding secondary branches separated by forward slashes. Ectopic ventral and dorsal branches in *Intu* mutant lungs are labeled with arrows and indicated in red font. L: lateral; M: medial; A: anterior; P: posterior. D: dorsal; V: ventral.

Figure 2. Cilia defects in *Intu* mutant lungs. Cilia were visualized through ARL13B immuno-fluorescence (red). Nuclei were shown with DAPI (blue). Dashed lines outline the epithelium (ep). me: mesenchyme. Ciliation frequency comparisons were made through unpaired, two-tailed *Student's* t-test assuming unequal variances. n= 3 wild type and 3 mutant lungs.

Figure 3. Compromised Hh signaling in *Intu* mutant lungs. (A, B) The levels of *Shh* expression were comparable between wild type (n=9) and *Intu* mutant (n=3) lungs. es: esophagus. (C-H) Reduced expression of *Ptch1* (n=3 wild type and 3 mutant), *Ptch1-lacZ* (n=5 wild type and 3 mutant) and *Gli1-lacZ* (n=3 wild type and 3 mutant) in *Intu* mutant lungs. (A-D) RNA in situ hybridization. (E-H) Xgal staining. All are ventral views at E12.5. (I) Quantitative RT-PCR revealed significant reduction of *Ptch1* and *Gli1* in E12.5 *Intu* mutant lungs (n=4) compared to both E11.5 (n=5) and E12.5 (n=3) wild type lungs. Comparisons were made through unpaired, two-tailed *Student's* t-test assuming unequal variances.

Figure 4. Hh signaling defects in *Intu* mutant lung explants. (A) SMO agonist (SAG) activated Hh signaling, leading to increased *Gli1-lacZ* expression (blue, Xgal stained) in E11.5 wild type

lung explants (n=4 control DMSO-treated and 4 SAG-treated), but not in *Intu* mutant lung explants (n= 4 DMSO-treated and 3 SAG-treated). (B) SAG activated *Ptch1-lacZ* expression (blue, Xgal stained) in E11.5 wild type lung explants (n=9 DMSO-treated and 6 SAG-treated), but not in *Intu* mutant lung explants (n= 3 DMSO-treated and 3 SAG-treated). (C) Immunofluorescence with a NKX2-1 antibody showed that SAG treatment promoted tubular morphogenesis and increased branching in wild type explants (n=10 DMSO-treated and 9 SAG-treated), but not in *Intu* mutant explants (n=6 DMSO-treated and 5 SAG-treated). (D) Quantification of branch tip numbers in various explants. ****: $p=5x\ 10^{-5}$. ns: p=0.7, Two-tailed, unpaired *Student's* t-tests assuming unequal variances. All explants were cultured for 48 hrs at 37℃, 5% CO_2.

Figure 5. Compromised GLI2 degradation and GLI3 processing in *Intu* mutant lungs. (A) Representative images of immunoblots for GLI2, GLI3 and β-tubulin. (B~E) Quantification of GLI2, GLI3FL, GLI3R normalized against β-tubulin, as well as the GLI3FL/GLI3R ratio. au: arbitrary units; *: p<0.05; **: p<0.01; ****: p<0.0001. ns: not significant; Two-tailed, unpaired *Student's* t-tests assuming unequal variances. n=16 E13.5 wild type and *Intu* mutant lungs, respectively, were lysed in 8 pools of 2 lungs each for this analysis.

Figure 6. Loss of *Gli2* exacerbates the *Intu* mutant lung defects. (A) Five lobes and extensive primary and secondary branches were present in E12.5 wild type lungs (n=12). (B) One lobe remained in each side of *Gli2* mutant lungs with limited secondary branches (n=6). (C) One lobe remained in each side of *Intu* mutant lungs with few primary branches (n=9). (D) A single patch of NKX2-1 expressing cells was present on the ventral side of *Gli2;Intu* double mutant foregut without side branches (n=5). Shown are ventral views of E12.5 lungs processed for NKX2-1 immunofluorescence to show lung branches.

Figure 7. Transcriptomic basis of the *Intu* mutant lung defects. RNA Sequencing was performed on E12.5 wild type (n=3) and *Intu* mutant (n=7, in three pools) left and right lungs separately. (A) A Principal Component Analysis of the sequencing results indicating the clear difference between wild type and *Intu* mutant lungs. It also shows a minor difference between the left and right wild type lungs that was diminished in *Intu* mutants. (B) Multiple Hh target genes including *Ptch1, Ptch2, Gli1* and *Hhip1*, were downregulated in *Intu* mutant lungs. (C) A volcano

plot showing Hh target genes and genes expressed in smooth muscles among downregulated genes in *Intu* mutant lungs. (D) A pathway enrichment analysis using g.Profiler indicated that genes involved in cytoskeleton, cell movement and proliferation, organ morphogenesis and Hh signaling were differentially expressed in *Intu* mutant lungs. (E) A heatmap showing the downregulation of smooth muscle specific genes in *Intu* mutant lungs.

Figure 8. Defective smooth muscle differentiation and IGF signaling in *Intu* mutant lungs. (A) *Foxf1* expression was significantly downregulated in E12.5 *Intu* mutant lungs. n=15 wild type and 6 mutant lungs for wholemount in situ hybridization. n=3 E11.5 wild type, 3 E12.5 wild type and 4 E12.5 *Intu* mutant lungs for RT-PCR analysis. **: $p<0.01$. Unpaired two-tailed *Student's* t-test assuming unequal variance. (B) Smooth muscle development was disrupted in E12.5 *Intu* mutant lungs indicated by reduced expression of smooth muscle actin (SMA, arrowheads). Lung tubules were labelled with NKX2-1, and nuclei were labelled with DAPI. n= 3 wild type and 3 mutant lungs. (C) *Igf1* expression was significantly reduced in *Intu* mutant lungs. n=15 wild type and 4 mutant lungs for wholemount in situ hybridization. n=3 E11.5 wild type, 3 E12.5 wild type and 4 E12.5 *Intu* mutant lungs for RT-PCR analysis. ns: $p>0.05$, **: $p<0.01$. Unpaired two-tailed *Student*'s t-test assuming unequal variance.

Figure 1

Click here to access/download;Figure;Figure 1 Intu lung morphology.jpg

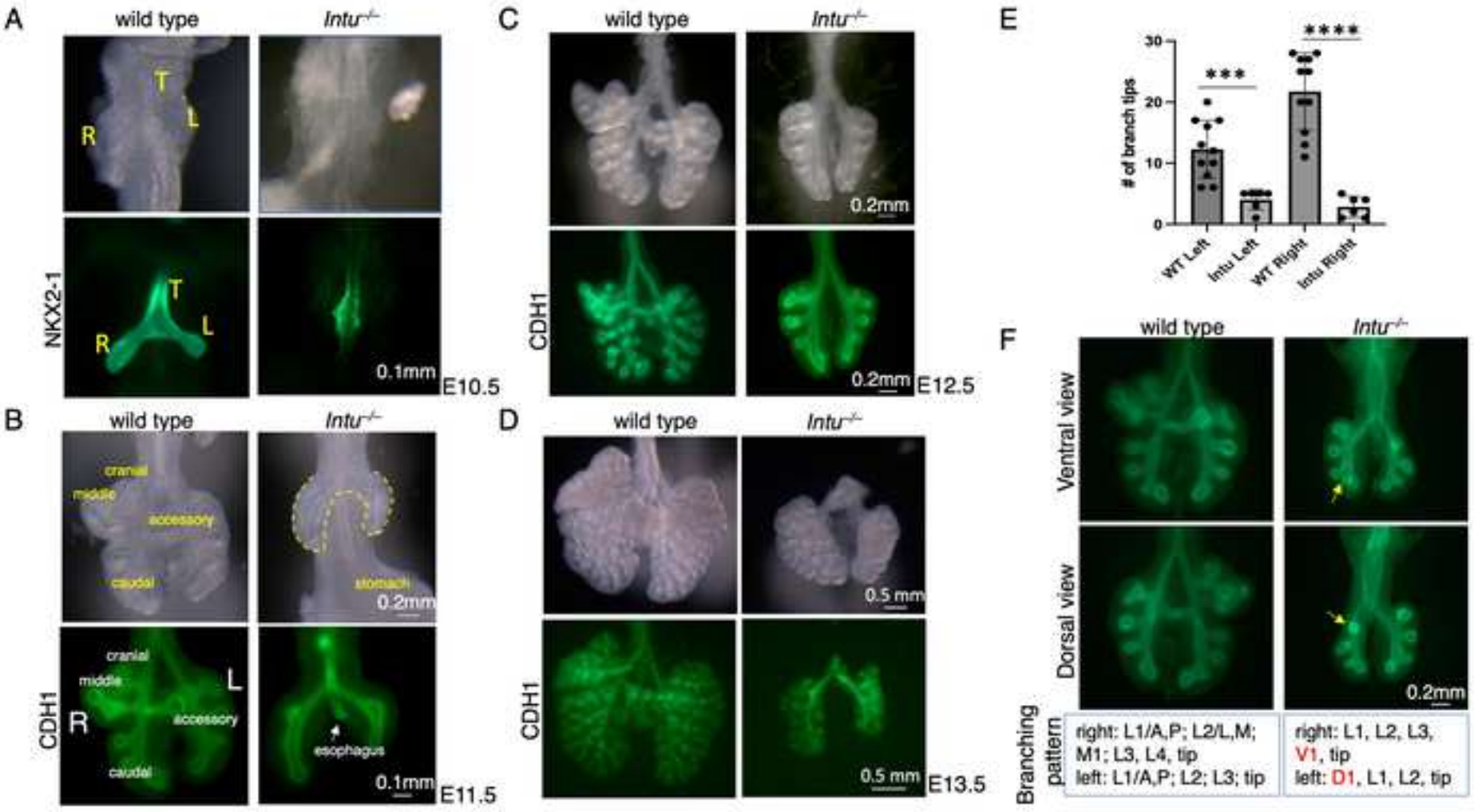

Figure 2

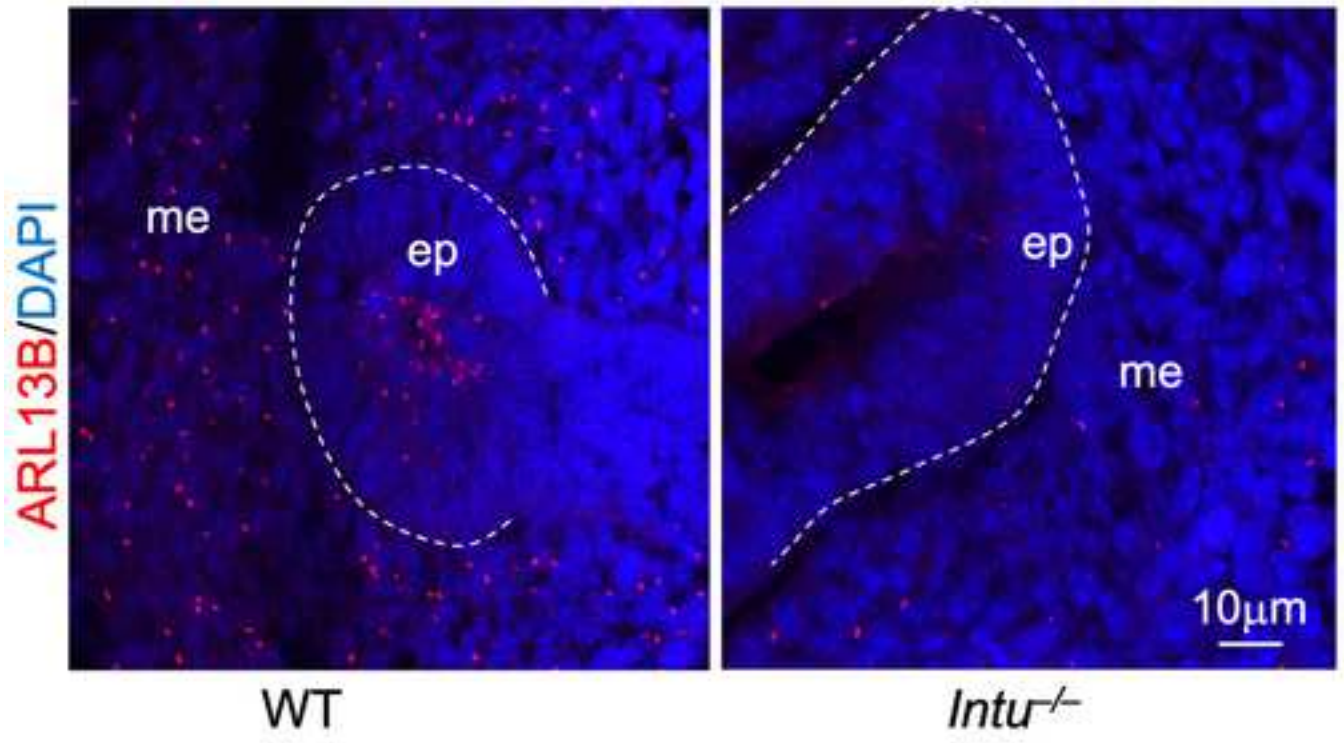

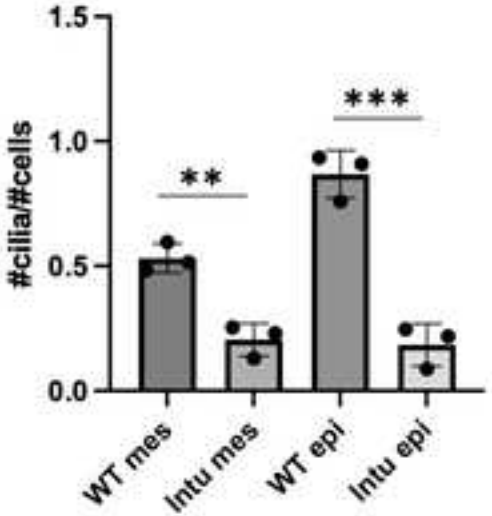

Figure 3

Click here to access/download;Figure;Figure 3 HH Signaling In Intu Lung.jpg

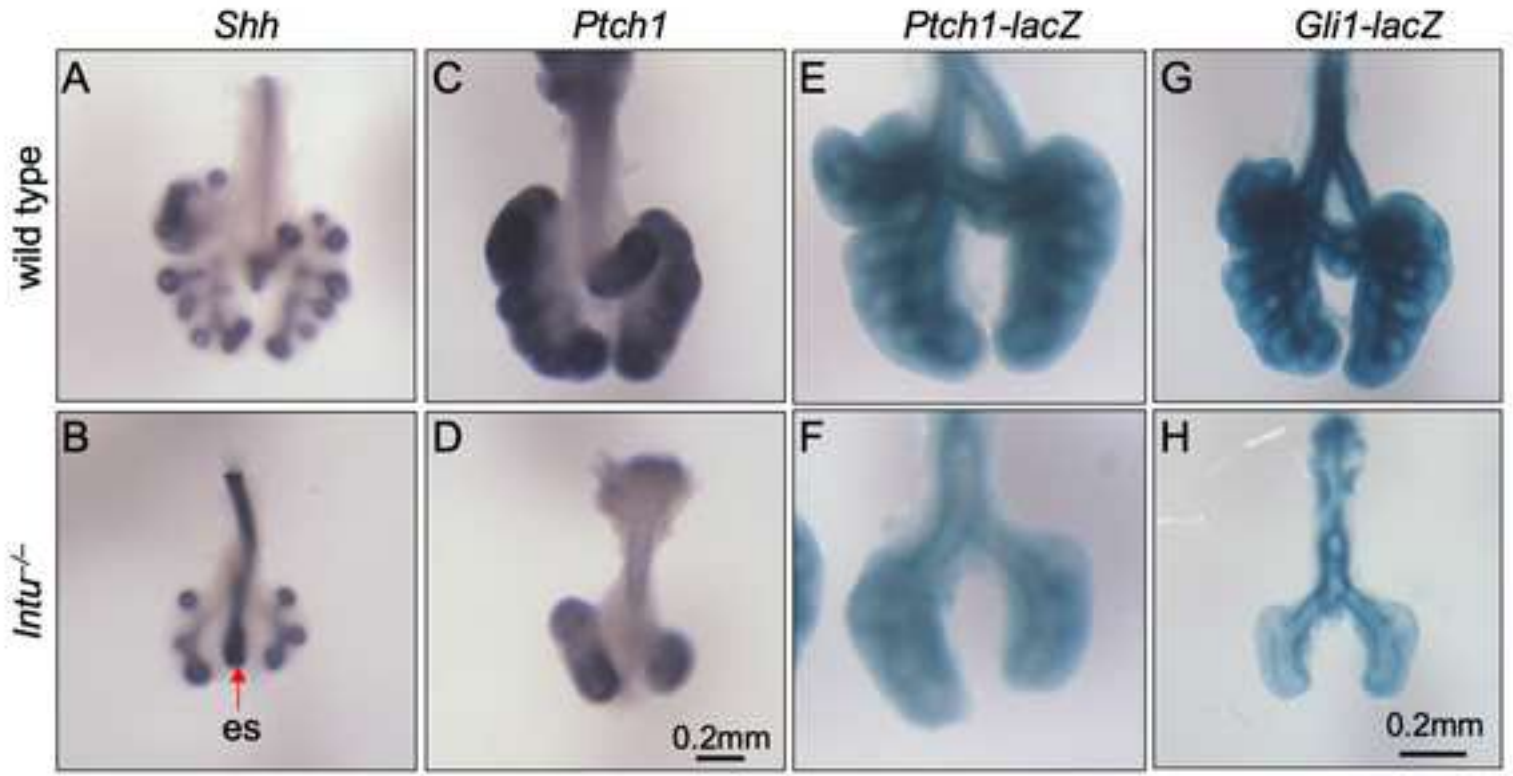

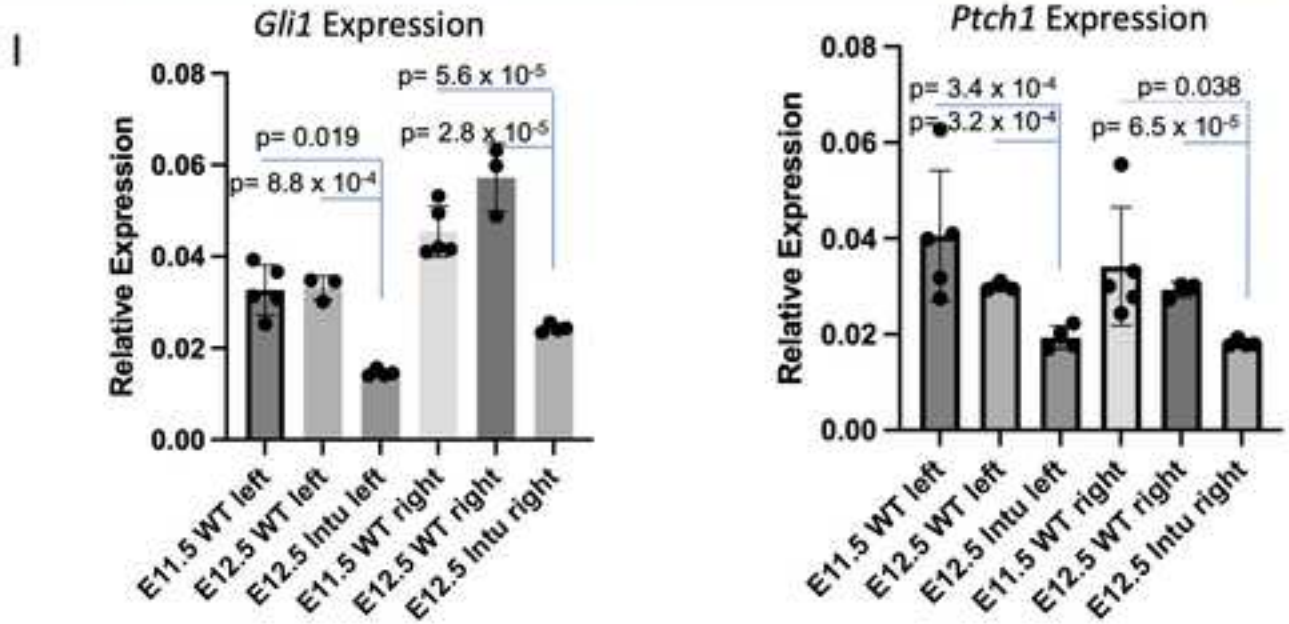

Figure 4

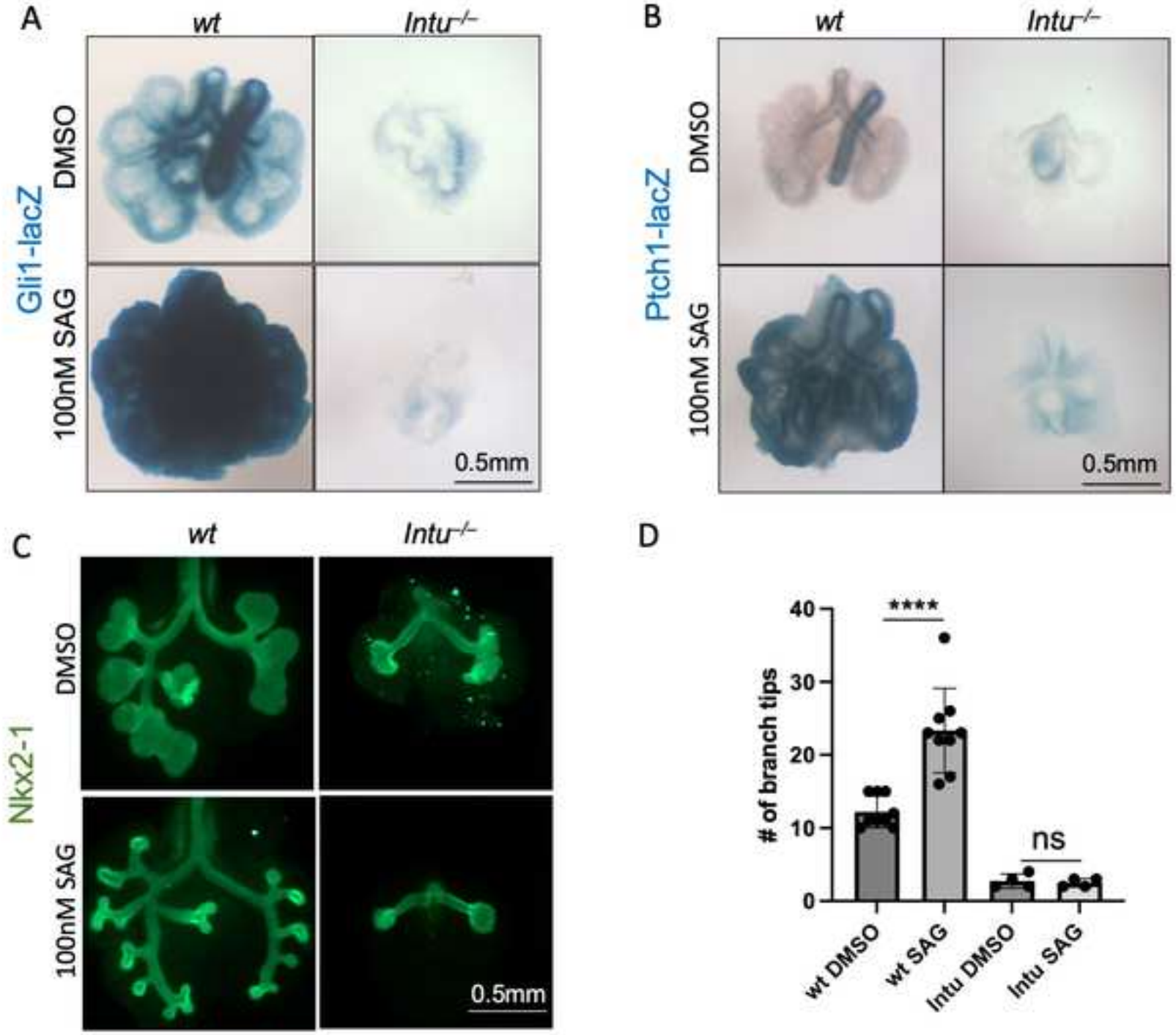

Figure 5

Click here to access/download;Figure;Figure 5 Gli Western.jpg

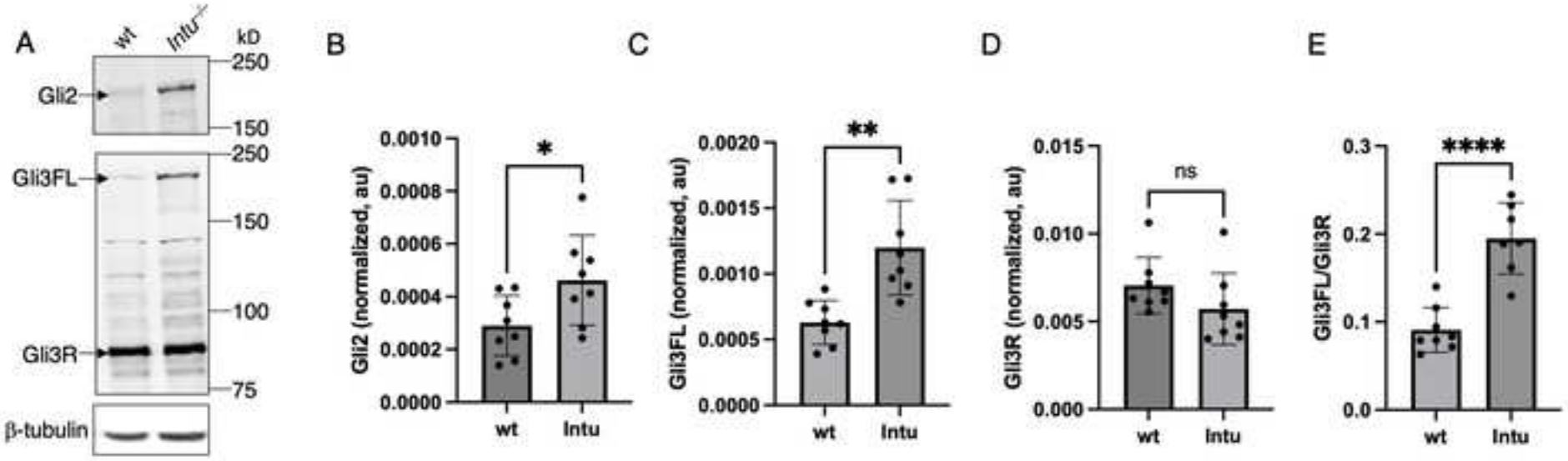

Figure 6

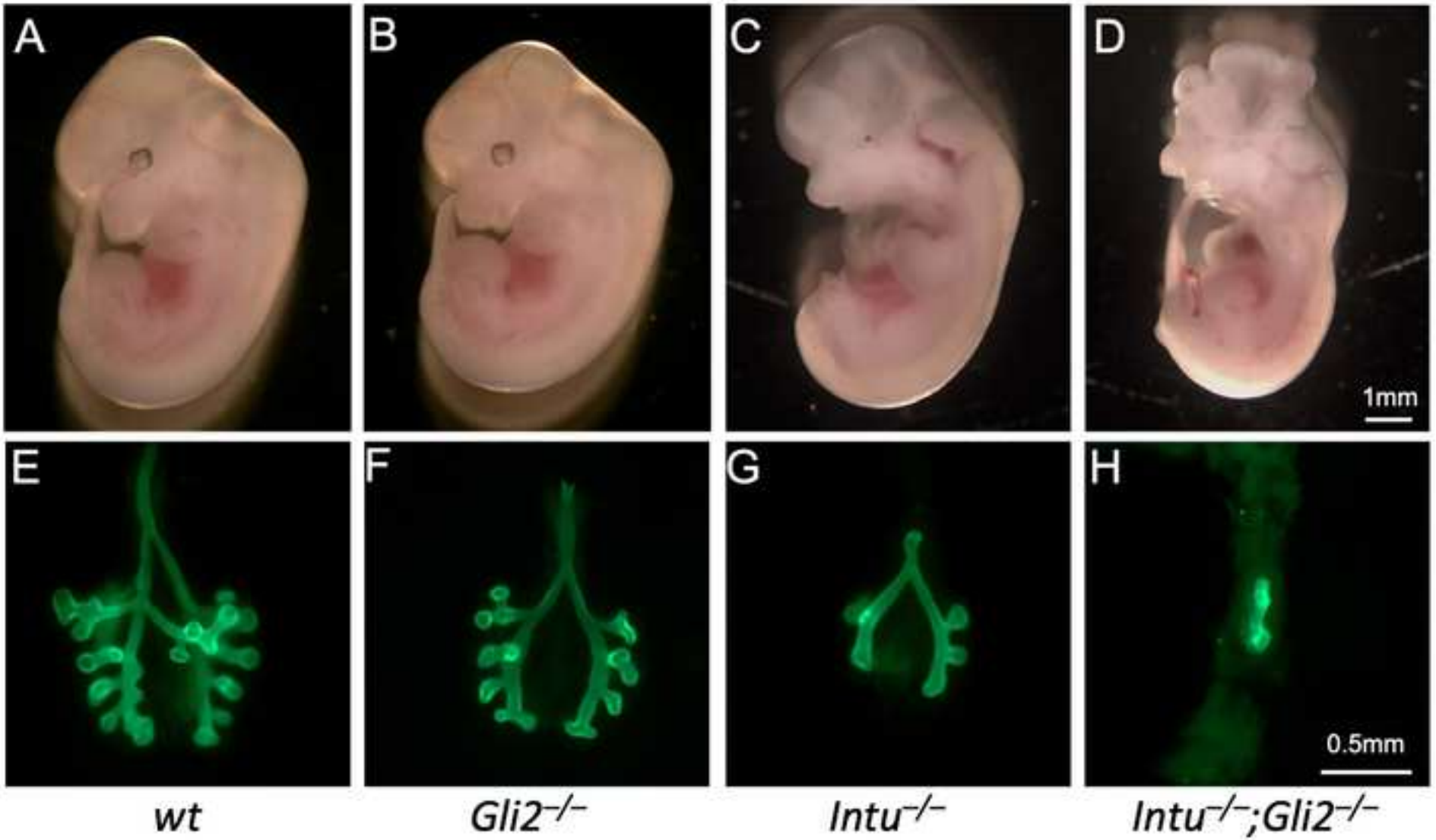

Figure 7

Click here to access/download;Figure;Figure 7 RNA seq.jpg

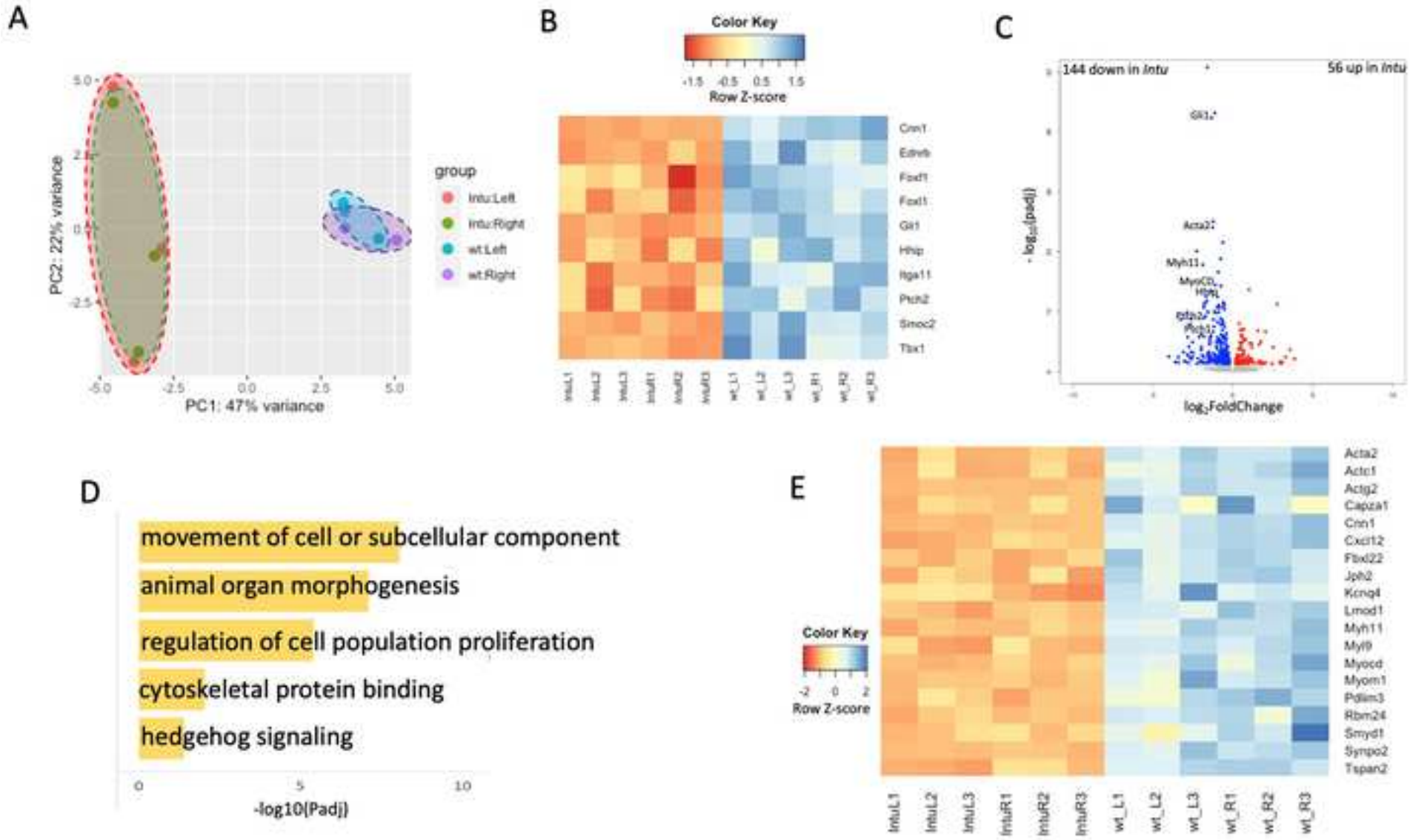

Figure 8